[American Journal of Science, Vol. 312, January, 2012, P. 1–21, DOI 10.2475/01.2012.01]

American Journal of Science

JANUARY 2012

TEMPERATURES AND FLUIDS ON FAULTS BASED ON CARBONATE CLUMPED–ISOTOPE THERMOMETRY

ERIKA M. SWANSON*,†, BRIAN P. WERNICKE*, JOHN M. EILER*, and STEVEN LOSH**

ABSTRACT. We present results from a carbonate clumped-isotope thermometric study of 42 carbonate samples collected within ~1 m or less of the Mormon Peak detachment, a large-slip Miocene normal fault in the Basin and Range province of southern Nevada. Samples include cataclastic rocks, narrow vein fillings and larger void-filling carbonates. Our results are consistent with earlier measurements of O and C isotopic ratios and fluid inclusion temperatures, and provide independent constraints on the isotopic composition and temperature of both syntectonic and post-tectonic pore waters. The results reveal a wide range of precipitation temperatures (24 to 137 °C) associated with deformation, and indicate that the pore waters were meteoric, with $\delta^{18}O$ as low as −11.6 permil (VSMOW) and $\delta^{13}C$ as low as −8.0 permil (VPDB). The results do not provide any direct evidence for high-temperature thermal decarbonation reactions (~500 to 800 °C) that are widely expected to result from flash heating along upper crustal faults, although they do not rule them out so long as recarbonation occurs at very low temperature, or the products of these reactions are volumetrically minor. The results are difficult to reconcile with recent suggestions that the detachment is the base of one or more catastrophically emplaced, surficial landslides. In concert with other lines of evidence, the data are most simply interpreted as recording deformation and precipitation events through a long history of slip, accompanied by relatively deep (> 3 km) circulation of meteoric pore waters along the detachment plane.

Key words: Fault rocks, Mormon Peak detachment, fluids, friction, and clumped isotopes

INTRODUCTION

Motion on large, upper crustal fault zones is governed in large part by the evolution of temperature and pore fluid pressure within cataclasites (for example Rice, 1992, 2006; Blanpied and others, 1998; de Lorenzo and Loddo, 2010; Goren and others, 2010; De Paola and others, 2011). However, observations that constrain the temperature of cataclastic deformation in natural faults, and the origin and evolution of syntectonic pore fluids, are relatively limited. Fault motion may occur under high enough temperature and pressure to generate frictional melting during slip, particularly in granitic rocks (Sibson, 1975; Hirose and Shimamoto, 2005), but evidence of such melting is not ubiquitous in exposed upper crustal fault zones. Recent studies have demonstrated the viability of using Ar-Ar dating of clay minerals in fault gouge to constrain the timing of fault slip, but this method is limited in its ability to resolve the thermal evolution (Haines and van der Pluijm, 2010; Duvall and others, 2011).

* Division of Geological and Planetary Sciences, California Institute of Technology, Pasadena, California 91125
** Department of Chemistry and Geology, Minnesota State University, Mankato, Minnesota 56001
† Corresponding author: eswanson@caltech.edu

Stable isotope and fluid inclusion studies have shed considerable light on both temperatures and sources of pore fluids in cataclasites and associated vein arrays in carbonates (for example McCaig and others, 1995; Losh, 1997; Hausegger and others, 2010). However, the stable isotopic studies are limited by the necessity of assuming the oxygen isotope composition of the pore waters in equilibrium with carbonate in order to determine temperature or, conversely, to assume temperature in order to reach conclusions regarding the isotopic compositions of waters. To overcome this limitation, we measured crystallization temperatures of fault rocks, vein arrays, and void fillings localized along a large-slip (>10 km) upper crustal fault zone, the Mormon Peak detachment in southern Nevada, using the carbonate clumped–isotope thermometer. Each clumped-isotope measurement independently constrains both the temperature and the C and O isotopic composition of carbonate, which in turn constrains the equilibrium O isotopic composition of co-existing fluid.

We chose the Mormon Peak detachment for study because it was previously the subject of detailed stable isotope and fluid inclusion studies (Losh, 1997; Diehl and others, 2010), and to test competing hypotheses for the origin of the detachment. The detachment is exposed over an area of 400 km^2 and has generally been interpreted as an upper crustal normal fault with ~20 km of slip, that initiated at a relatively constant dip of 17 to 25° through the upper 8 km of the crust (Wernicke and others, 1985; Axen and others, 1990). Anderson and others (2010) and Diehl and others (2010) also interpret the detachment as a low-angle normal fault, but suggest, on the basis of abundant dissolution and collapse features in the upper plate, that the bulk of the upper-plate thinning is due to dissolution by a mixture of meteoric and CO_2-rich mantle fluids concentrated along the fault zone. Citing mechanical difficulties with both the initiation and active slip along low-angle normal faults in the upper crust, as well as other evidence, other investigators have interpreted the detachment as the base of a system of catastrophically emplaced landslide deposits (for example Walker and others, 2007), possibly accompanied by high-temperature thermal decomposition of carbonate (for example Anders and others, 2006).

In addition to their implications for upper crustal fault mechanics, the data presented below represent, to our knowledge, the first application of carbonate clumped-isotope thermometry to a problem in structural geology, and thus allow an assessment of its viability as a new tool.

CLUMPED-ISOTOPE THERMOMETRY

Clumped isotope thermometry is a relatively new technique used to determine the crystallization temperature of carbonate minerals. It takes advantage of the temperature dependence of the degree to which the heavy isotopes ^{13}C and ^{18}O bond to each other (Eiler, 2007). This effect can be described as an exchange reaction with the form:

$$Ca^{13}C^{16}O_3 + Ca^{12}C^{18}O^{16}O_2 = Ca^{13}C^{18}O^{16}O_2 + Ca^{12}C^{16}O_3$$

The forward reaction causes "clumping" of the heavy isotopes. The extent to which this forward reaction is favored depends on the balance between the lower vibrational energy of the $^{13}C—^{18}O$ bond and the entropy of the system, as described in Schauble and others (2006). At higher temperatures, a more random distribution is favored, whereas at lower temperatures, clumping is preferred. This degree of ordering is set during crystallization at temperatures less than ~200 to 300 °C, and readily modified by intracrystalline diffusion at higher temperatures (Eiler, 2007).

Using the sample preparation and analysis techniques described in Huntington and others (2009), the samples were reacted with phosphoric acid at 90 °C to produce CO_2 gas, which was then cleaned by established cryogenic and gas chromatographic

methods and measured for masses 44–49 using a Finnegan 253 gas source mass spectrometer. The measured mass 47, which consists principally of $^{13}C^{18}O^{16}O$, but also minor quantities of $^{12}C^{18}O^{17}O$ and $^{13}C^{17}O_2$, is compared to that expected for a stochastic distribution, and the difference is denoted as Δ_{47}, in units of permil (Eiler, 2011). The raw Δ_{47} values are standardized by comparison to CO_2 gases heated to achieve a nearly stochastic distribution, and then corrected for temperature-dependent fractionation during acid digestion. The corrected Δ_{47} values are empirically related to temperature using experimental data from natural and synthetic calcites, aragonites and dolomites (Bonifacie and others, in preparation; Bonifacie and others, 2011).

One-sigma standard errors, based on the cumulative results of 8 acquisitions of 7 cycles per acquisition, range from 0.0005 permil to 0.0068 permil (averaging 0.002‰) in the carbon and oxygen isotope measurements, and from 0.004 permil to 0.021 permil (averaging 0.010‰), for Δ_{47}. These errors in Δ_{47} propagate into errors in temperature of ±2 to 8 °C (averaging ±3.4 °C) for the "cold suite" samples, and ±2 to 12 °C (averaging ±6.4 °C) for the "warm suite" samples, as defined below. These errors are comparable to the variation in temperatures that result from different calibration curves through the high-temperature data.

GEOLOGIC SETTING AND SAMPLE DESCRIPTIONS

The Mormon Peak detachment is an extensively exposed low-angle slip surface, active during middle Miocene extension in the Basin and Range province (Wernicke and others, 1985; Axen and others, 1990; fig. 1A). The footwall is a gently east-tilted crustal section through the frontal decollement zone of the Sevier fold-and-thrust belt, with approximately 8 km of pre-tilt structural relief (figs. 1B and 1C). The footwall of the detachment is unmetamorphosed and relatively intact structurally, and includes a thrust plate of Cambrian strata structurally overlying sub-thrust Cambrian through Mississippian strata resting nonconformably on early Proterozoic basement. Cambrian through Middle Devonian strata are predominantly dolostone, whereas Upper Devonian and younger strata are primarily limestone, each with relatively minor amounts of chert and siliciclastic strata. In eastern areas of exposure, the detachment cuts across Middle and Upper Cambrian strata of the thrust allochthon. The detachment truncates the thrust, such that in western areas of exposure, the footwall includes only sub-thrust rocks (fig. 1).

The hanging wall of the detachment (fig. 1C) consists of both east- and west-tilted normal fault blocks composed of Cambrian through Permian carbonates derived from the thrust allochthon, locally overlain by late Oligocene to middle Miocene (*ca.* 23-14 Ma) volcanic and sedimentary strata, all displaced westward relative to footwall rocks (Wernicke and others, 1985; Anderson and others, 2010). Where present, Tertiary strata are generally concordant with the underlying Paleozoic rocks. The structural depth of the base of hanging wall blocks prior to faulting and tilting was, therefore, not significantly greater than the total stratigraphic thickness of Tertiary and Paleozoic units, which is about 2000 m (fig. 1B).

Exposures of the detachment span an east-west distance of more than 20 km, corresponding to footwall paleodepths of ~2 to 8 km. We collected samples from 4 locations relatively evenly spaced across this transect (fig. 1A), generally within 1 m of the detachment plane. The samples include a variety of slip-related features (for example Anders and others, 2006), including breccias, fault gouge, veins, and void fills (figs. 2 and 3). In addition, we collected host rock samples from Cambrian strata 250 to 300 m structurally below the detachment. All samples were thin sectioned and analyzed petrographically. A subset of these (6 samples) containing very fine-grained material were analyzed using a scanning electron microscope. The breccia samples include clasts of host rock large enough to sample separately from the matrix, ranging from 5

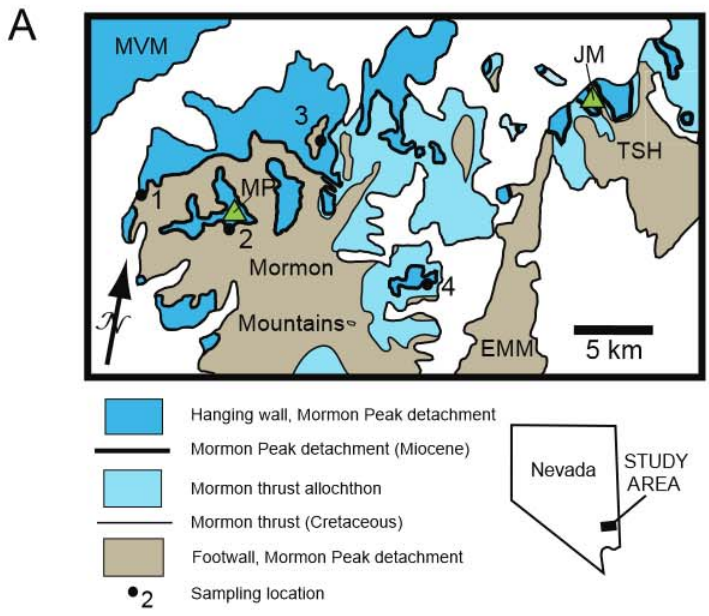

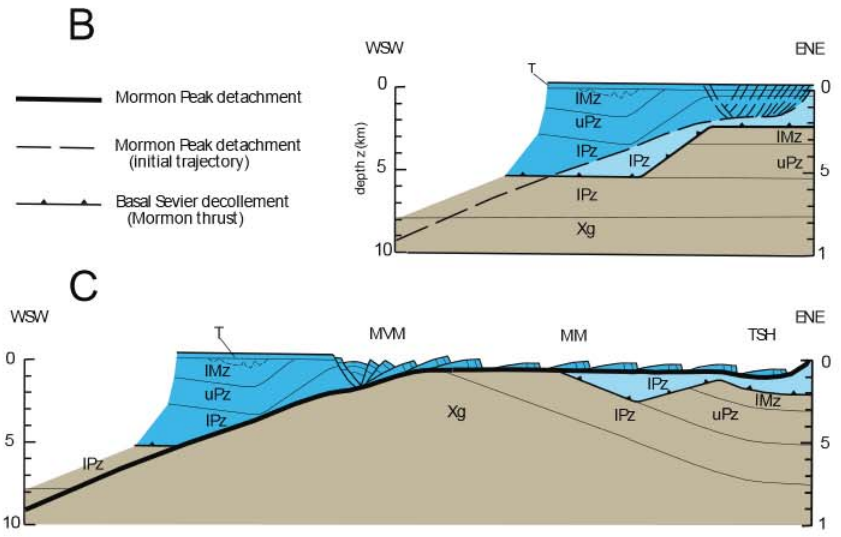

Fig. 1. Simplified structural map and cross-sectional reconstructions outlining the geology of the field site. (A) Map showing sample locations along the Mormon Peak detachment. (B) Reconstruction showing pre-extension position of units and the Mormon thrust. (C) Simplified cross-section of field area (subsequent deformation accommodated along the Tule Springs detachment is removed). EMM, East Mormon Mountains; TSH, Tule Springs Hills; MVM, Meadow Valley Mountains; MP, Mormon Peak; JM, Jumbled Mountain; MM, Mormon Mountains. Rocks units on (B) and (C): Xg, early Proterozoic crystalline rocks; lPz, lower Paleozoic stratified rocks (Cambrian to Devonian); uPz, upper Paleozoic stratified rocks (Carboniferous and Permian); lMz, lower Mesozoic stratified rocks (Triassic); T, Tertiary stratified rocks. (B) and (C) have no vertical exaggeration. Sample locations: Site 1, 36.9772°N, −114.5684°E; Site 2, 36.9642°N, −114.5098°E; Site 3, 37.0277°N, −114.4505°E; Site 4, 36.9576°N, −114.3654°E.

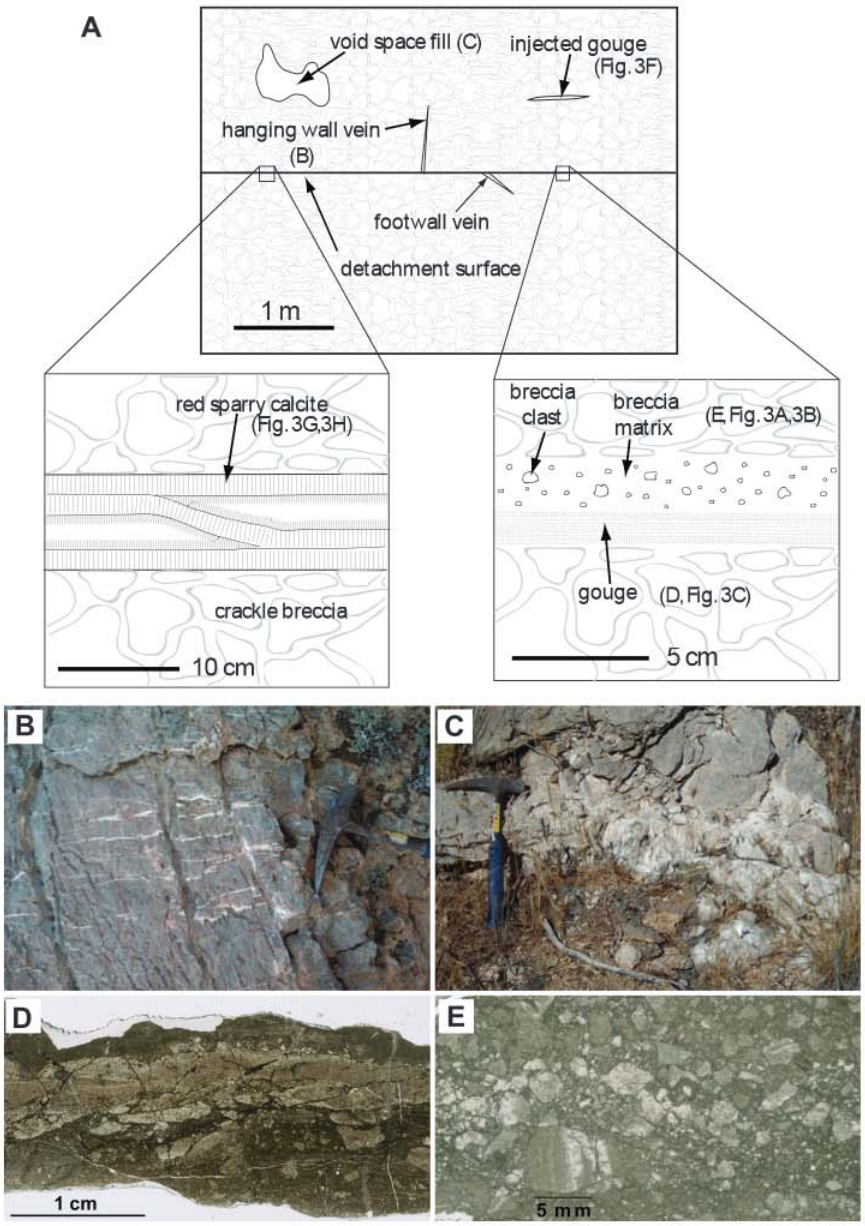

Fig. 2. Schematic diagram showing spatial relationships of various sample types with respect to the detachment, as well as photographs of the textures in the warm suite of samples. (A) Diagram of the fault zone at three different scales, showing locations of different textures relative to the detachment plane. The size of the veins are enlarged for visibility, the other features are approximately to scale. The structure within the red sparry calcite is significantly simplified. (B) Photo of hanging wall host rock and veins, hammer head is 28 cm long. (C) Outcrop photograph of void-filling calcite spar (white area with irregular boundary) in Ordovician host dolostone (medium gray), hammer head is 28 cm long. (D) Photomicrograph of fault gouge from the detachment surface, in plane polarized light. The top dark layer is nearly pure dolomite, the middle layer (light brown) is silicified dolomite with iron oxides, and the lower dark brown layer is a breccia with both calcite and dolomite. (E) Fault breccia showing clasts of host dolostone.

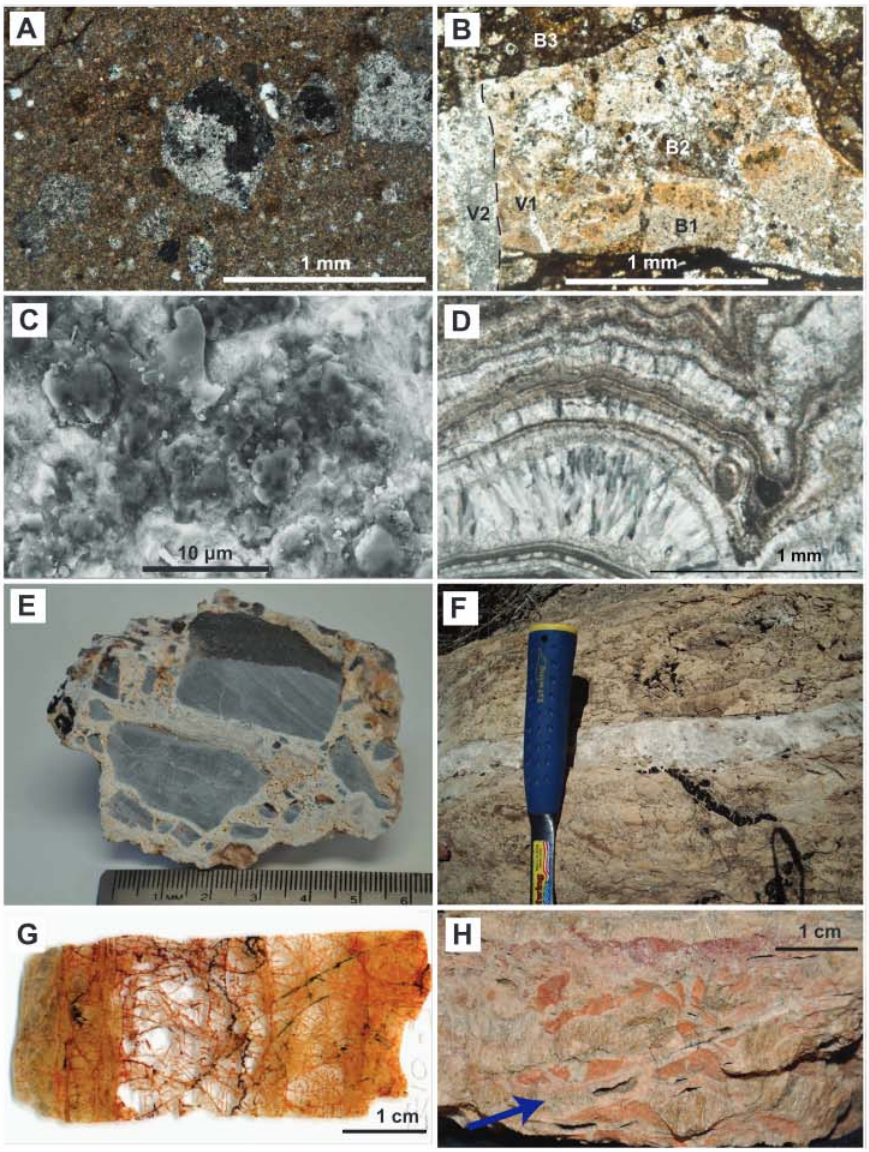

Fig. 3. (A) Photomicrograph of the "spar breccia" texture of sample ES10-27, showing a calcite spar clast (center) within a breccia, with crossed polars. The analyzed clast for this sample was about 8 mm in diameter. (B) Photomicrograph with plane polarized light of a breccia interpreted to exhibit a 5-event history, beginning with brecciation event B1 (oldest breccia) sitting in event B2 matrix, again overprinted by B3 (most recent matrix); calcite microvein event V1 occurred after B1 and before B3; microvein event V2 postdates B3. (C) SEM image of fault-plane gouge sample (ES10-23) showing variation in dolomite grain size from <0.1 µm up to 5 µm, with a small fraction of sub-micron, quasi-spherical grains in the center-right portion of the image. (D) Photomicrograph of isopachous cement, with crossed polars. (E) Hand sample of calcrete breccia, with clasts of Devonian limestone. (F) Outcrop photograph of injected gouge (white layer across center of image), hammer handle is 28 cm long. (G) Photomicrograph of red spar under reflected light. Thin section was made perpendicular to the detachment plane (vertical here). (H) Hand sample of the red sparry calcite, with lenses of spar (beige areas) interspersed with fine-grained mixtures of calcite and iron oxides (orange areas), and spar-lined fractures (along blue arrow). Sample taken from just above detachment plane, with the long axis (horizontal) parallel to the detachment.

Table 1

Summary of isotopic results, where $\delta^{13}C$ is with respect to VPDB, and $\delta^{18}O$ is with respect to VSMOW

[illegible]	[illegible]	[illegible]	[illegible]	[illegible]	[illegible]	[illegible]	[illegible]
[illegible]	[illegible]	[illegible]	[illegible]	[illegible]	[illegible]	[illegible]	[illegible]
[illegible]	[illegible]	[illegible]	[illegible]	[illegible]	[illegible]	[illegible]	[illegible]
[illegible]	[illegible]	[illegible]	[illegible]	[illegible]	[illegible]	[illegible]	[illegible]
[illegible]	[illegible]	[illegible]	[illegible]	[illegible]	[illegible]	[illegible]	[illegible]
[illegible]	[illegible]	[illegible]	[illegible]	[illegible]	[illegible]	[illegible]	[illegible]
[illegible]	[illegible]	[illegible]	[illegible]	[illegible]	[illegible]	[illegible]	[illegible]
[illegible]	[illegible]	[illegible]	[illegible]	[illegible]	[illegible]	[illegible]	[illegible]
[illegible]	[illegible]	[illegible]	[illegible]	[illegible]	[illegible]	[illegible]	[illegible]
[illegible]	[illegible]	[illegible]	[illegible]	[illegible]	[illegible]	[illegible]	[illegible]
[illegible]	[illegible]	[illegible]	[illegible]	[illegible]	[illegible]	[illegible]	[illegible]
[illegible]	[illegible]	[illegible]	[illegible]	[illegible]	[illegible]	[illegible]	[illegible]
[illegible]	[illegible]	[illegible]	[illegible]	[illegible]	[illegible]	[illegible]	[illegible]
[illegible]	[illegible]	[illegible]	[illegible]	[illegible]	[illegible]	[illegible]	[illegible]
[illegible]	[illegible]	[illegible]	[illegible]	[illegible]	[illegible]	[illegible]	[illegible]
[illegible]	[illegible]	[illegible]	[illegible]	[illegible]	[illegible]	[illegible]	[illegible]
[illegible]	[illegible]	[illegible]	[illegible]	[illegible]	[illegible]	[illegible]	[illegible]
[illegible]	[illegible]	[illegible]	[illegible]	[illegible]	[illegible]	[illegible]	[illegible]
[illegible]	[illegible]	[illegible]	[illegible]	[illegible]	[illegible]	[illegible]	[illegible]
[illegible]	[illegible]	[illegible]	[illegible]	[illegible]	[illegible]	[illegible]	[illegible]
[illegible]	[illegible]	[illegible]	[illegible]	[illegible]	[illegible]	[illegible]	[illegible]
[illegible]	[illegible]	[illegible]	[illegible]	[illegible]	[illegible]	[illegible]	[illegible]
[illegible]	[illegible]	[illegible]	[illegible]	[illegible]	[illegible]	[illegible]	[illegible]
[illegible]	[illegible]	[illegible]	[illegible]	[illegible]	[illegible]	[illegible]	[illegible]
[illegible]	[illegible]	[illegible]	[illegible]	[illegible]	[illegible]	[illegible]	[illegible]
[illegible]	[illegible]	[illegible]	[illegible]	[illegible]	[illegible]	[illegible]	[illegible]
[illegible]	[illegible]	[illegible]	[illegible]	[illegible]	[illegible]	[illegible]	[illegible]
[illegible]	[illegible]	[illegible]	[illegible]	[illegible]	[illegible]	[illegible]	[illegible]
[illegible]	[illegible]	[illegible]	[illegible]	[illegible]	[illegible]	[illegible]	[illegible]
[illegible]	[illegible]	[illegible]	[illegible]	[illegible]	[illegible]	[illegible]	[illegible]
[illegible]	[illegible]	[illegible]	[illegible]	[illegible]	[illegible]	[illegible]	[illegible]
[illegible]	[illegible]	[illegible]	[illegible]	[illegible]	[illegible]	[illegible]	[illegible]
[illegible]	[illegible]	[illegible]	[illegible]	[illegible]	[illegible]	[illegible]	[illegible]
[illegible]	[illegible]	[illegible]	[illegible]	[illegible]	[illegible]	[illegible]	[illegible]
[illegible]	[illegible]	[illegible]	[illegible]	[illegible]	[illegible]	[illegible]	[illegible]
[illegible]	[illegible]	[illegible]	[illegible]	[illegible]	[illegible]	[illegible]	[illegible]
[illegible]	[illegible]	[illegible]	[illegible]	[illegible]	[illegible]	[illegible]	[illegible]
[illegible]	[illegible]	[illegible]	[illegible]	[illegible]	[illegible]	[illegible]	[illegible]
[illegible]	[illegible]	[illegible]	[illegible]	[illegible]	[illegible]	[illegible]	[illegible]
[illegible]	[illegible]	[illegible]	[illegible]	[illegible]	[illegible]	[illegible]	[illegible]
[illegible]	[illegible]	[illegible]	[illegible]	[illegible]	[illegible]	[illegible]	[illegible]
[illegible]	[illegible]	[illegible]	[illegible]	[illegible]	[illegible]	[illegible]	[illegible]
[illegible]	[illegible]	[illegible]	[illegible]	[illegible]	[illegible]	[illegible]	[illegible]

%Dolomite is the dolomite fraction of the carbonate, the rest being calcite. The sample names reflect the sample preparation method, with T referring to the track (microdrilling location), C referring to chip, and M referring to mortar and pestle powder. Samples without an additional letter are drilled. S refers to sample, and is only used for replicate analyses of a single powder. See figure 1 for site locations.

to 8 mm in diameter. Breccia clasts mostly consist of dolostone, and often showed the fine-grained textures typical of the host rock Paleozoic formations (fig. 2E). Important exceptions include one sample (ES10-27, table 1) that contains clasts of coarse calcite spar typical of veins and void fills (fig. 3A), and other samples that contain clasts that are themselves breccia (fig. 3B). The latter samples record multiple episodes of fracturing and vein filling (Anderson and others, 2010; Diehl and others, 2010;

compare with Anders and others, 2006). In a single thin section, as many as five discrete fragmentation and veining events may be observed (fig. 3B). The breccia matrix samples are bulk measurements of the fine-grained material, with highly variable grain size ranging from ~1 mm to sub-micron scale.

Gouge samples include one from a centimeter-thick layer of ultra-fine-grained material (from <0.1 μm to 10 μm) directly on the detachment slip surface (figs. 2D and 3C) and a mineral assemblage that includes calcite, dolomite, quartz, and iron oxide. An SEM image of a small portion of the gouge sample shows a number of micron-scale, quasi-spherical grains of similar geometry and scale to clusters of calcium oxide grains observed in frictional decarbonation experiments (compare with fig. 13D in Han and others, 2010). The texture is not ubiquitous, and no evidence of magnesium or calcium oxide, or their hydrated forms, is present in any of the analyzed gouges. A second sample is from an ultra-fine-grained, porous layer about 5 cm thick that we interpret to have been injected upward into the hanging wall, ~1 m above the detachment plane (fig. 3F). Although this layer could not be traced directly to the slip plane, it presumably intersects the detachment below the exposed plane of outcrop.

Vein material was collected from millimeter-scale calcite veins in both the hanging wall and footwall. The void fill samples consist of clean, sparry calcite from large (>50 cm diameter) vugs with irregular boundaries, located approximately 1 m above the detachment surface (fig. 2C). Red-hued calcite spar is locally found along and near the detachment surface, and exhibits only mild strain and multiple episodes of precipitation (figs. 3G and 3H), which we interpret to be post-tectonic. One of the breccia samples is composed of Devonian limestone clasts cemented with a calcrete matrix (fig. 3E), which we interpret to be the result of soil precipitation into void space created by post-tectonic cavity collapse. One sample exhibits micro-layered isopachous calcite cement growing into small void spaces (fig. 3D), and probably formed under near-surface conditions.

ISOTOPIC DATA

Forty-two samples were analyzed for carbon, oxygen, and clumped-isotopic compositions, in order to determine fluid sources and temperatures (table 1; a full data table may be found in the Appendix, table A1). Powders were most often obtained by microdrilling, using a 0.5 mm drill bit, ~10 mg of carbonate from either saw-cut or split samples. Accordingly, features smaller than 5 mm are too small to sample separately using this technique. To test for possible effects of sample preparation methods, a few samples were analyzed as chips or ground with a mortar and pestle. The results indicate that no significant differences in recorded temperature are observed from using different methods (table 1). For texturally complex samples, we drilled the opposing surfaces of the saw cuts from which the thin sections were taken, in order to assure precise correspondence between analyte and petrographic observations. Powders were analyzed according to procedures described by Huntington and others (2009). All stated carbon isotopic ratios are $\delta^{13}C$ with respect to Vienna Pee Dee Belemnite (VPDB), and oxygen isotopic ratios are $\delta^{18}O$ with respect to Vienna Standard Mean Ocean Water (VSMOW). Fractionation factors used to calculate the $\delta^{18}O$ composition of pore waters are from O'Neil and others (1969) and Vasconcelos (2005). Acid digestion fractionation factors were taken from Guo and others (2009) and Rosenbaum and Sheppard (1986). For mixed calcite-dolomite samples, all calculations were done for both end members of pure calcite and pure dolomite, and the $\delta^{18}O$ carbonate and $\delta^{18}O$ water values reflect a weighted average based on estimates of the calcite/dolomite ratios.

Calcite/dolomite ratios of fine-grained samples were estimated from both x-ray diffraction (xrd) analyses and visual estimates using SEM images (table 1). The xrd data only provided a semi-quantitative ratio, and analyses of samples with known ratios

were performed to evaluate accuracy. For all but sample BW-83-X, xrd analyses agreed well with our visual estimates. For BW-83-X, the dolomite content was highly variable across the thin section (from 50-95%), and thus we use the xrd value (90%) here due to its textural similarity to the powder analyzed for its clumped-isotope composition. The visual estimates were made from SEM images near the microdrilling site, estimating relative areas of their respective emission intensities, with spot checks using EDS to confirm the composition of each phase. Host rock, void-fill, and vein mineralogies (that is, samples without mixed compositions) were reacted with dilute hydrochloric acid to confirm our calcite versus dolomite determination based on texture. Errors in xrd data were generally less than 20 percent, an amount that could change the $\delta^{18}O$ of carbonate by 0.5 permil, and the $\delta^{18}O$ of water by 1 permil. Temperatures calculated from clumped isotope measurements are not noticeably affected by the proportion of calcite versus dolomite.

The different rock types show distinct clusters in various two-dimensional plots (for example $\delta^{13}C$ of carbonate vs. $\delta^{18}O$ of carbonate, temperature vs. the calculated $\delta^{18}O$ of water, *et cetera;* figs. 4 and 5). The host rocks, as well as almost all the breccia clasts, have $\delta^{18}O$ values of 22 to 26 permil, $\delta^{13}C$ values of -2 to 2 permil, precipitation temperatures of 80 to 130 °C, and calculated fluid $\delta^{18}O$ values of 3 to 6 permil. These values are consistent with primary deposition in a marine environment on a Paleozoic continental shelf, followed by recrystallization during burial diagenesis in a relatively closed (that is, fluid poor) environment. The gouge sample from the detachment surface has similar isotopic composition and apparent temperature to the host rock, consistent with it consisting of finely ground wall rock, although the texture and mineralogy described above indicate a more complex evolution. Nearly all breccia matrix analyses have $\delta^{18}O$ compositions of 15 to 20 permil, intermediate between host rock and the much lighter void fills discussed below. Carbon isotope ratios and calculated temperatures are similar to the host rock and void fill samples. The breccia matrix samples may thus be mechanical mixtures of these two rock types, although the presence of calcite precipitated from heavier, more exchanged waters (for example Losh, 1997) cannot be ruled out. Sample ES10-27 is the only exception to this trend, and is discussed further below.

The void-filling sparry calcite samples have $\delta^{18}O$ values of 8 to 10 permil, $\delta^{13}C$ values of -0.5 to 1.5 permil, and temperatures of 70 to 115 °C. One of the hanging wall veins shows similar values. The water in equilibrium with these samples at their growth temperatures has a calculated oxygen isotope composition of about -9 ± 3 permil (table 1). These values are consistent with precipitation from relatively warm, subsurface meteoric water, at temperatures broadly comparable to those at which host rocks underwent diagenesis. We emphasize, however, that these sparry void-filling carbonates (1) are not observed in host rocks away from the detachment zone, and (2) grew in equilibrium with much lower $\delta^{18}O$ waters than co-existed with the host rocks at these temperatures (3-6‰), as illustrated in figure 5B.

The footwall vein sample has a $\delta^{18}O$ value of 16.1 permil, $\delta^{13}C$ value of -2.7 permil, a temperature of 144 °C, and precipitated from water with a $\delta^{18}O$ value of 3.4 permil. This vein precipitated from a warm fluid that is heavier than meteoric waters, perhaps due to a higher degree of exchange with the host rocks, which have roughly the same fluid $\delta^{18}O$ value as the vein (fig. 5B). The heavier fluid $\delta^{18}O$ composition of the host rocks most likely reflects the composition of the fluid during burial diagenesis and dolomitization of the Paleozoic shelf deposits. The large difference in the carbonate $\delta^{18}O$ value between the vein and the host (fig. 5A) is mostly due to the difference in carbonate-water fractionation factors of calcite (the vein) and dolomite (the host rock).

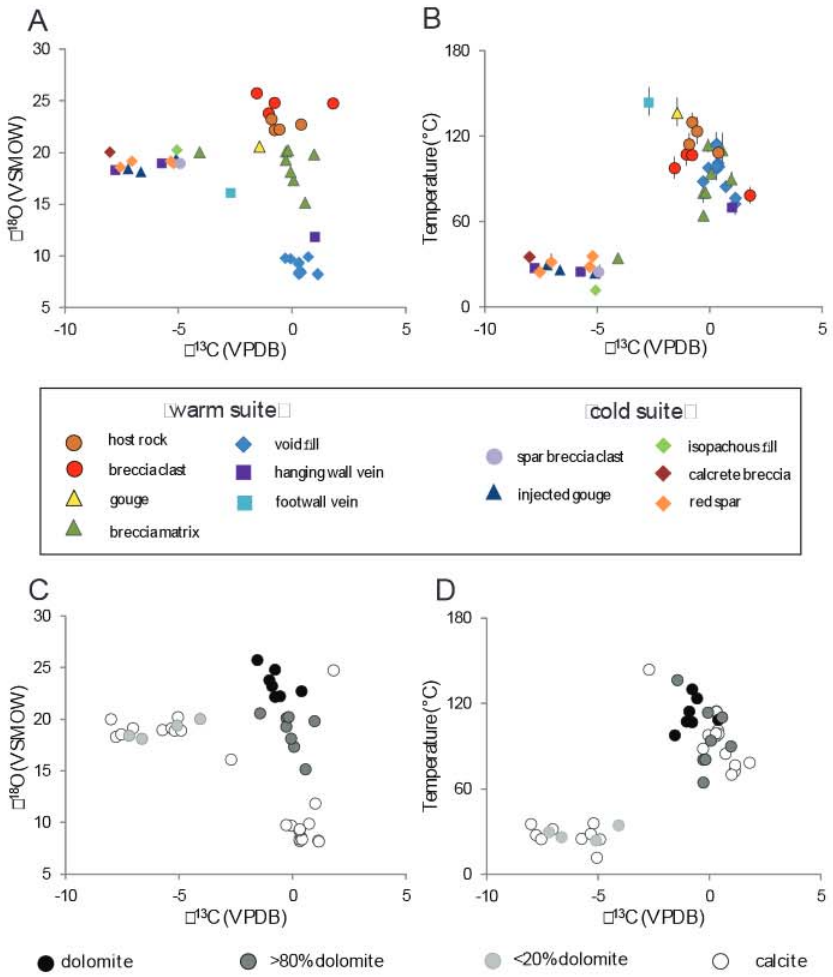

Fig. 4. Plots showing stable isotopic data and temperatures, keyed by texture (A and B) or by mineralogy (C and D). Textures in legend are grouped by approximate temperature. Errors in temperature are 1 sigma. One-sigma errors in oxygen and carbon isotopic compositions are smaller than the symbol size. Plot (B) shows the distinct difference in both carbon composition and temperature between earlier "warm-suite" compositions and later "cold-suite" ones, with no overlap in either domain.

The remaining samples are compositionally similar to each other, but yield distinctly lower temperatures and lighter carbon than the other samples (fig. 4B), and we will thus refer to the former as the "cold suite," and to the latter as the "warm suite" (figs. 4 and 5). The cold suite includes the lowermost 12 samples on table 1, and exhibits a wide range of textures, including (1) injected gouge (fig. 3F), (2) spar-clast breccia (both clast and matrix, fig. 3A), (3) red sparry calcite (figs. 3G and 3H), (4) calcrete-cemented breccias (fig. 3E), and (5) isopachous void fill samples (fig. 3D), in addition to two of the vein samples. These samples have carbonate $\delta^{18}O$ values of 18 to 21 permil, $\delta^{13}C$ values of −8 to −5 permil, temperatures of only 12 to 36 °C, and

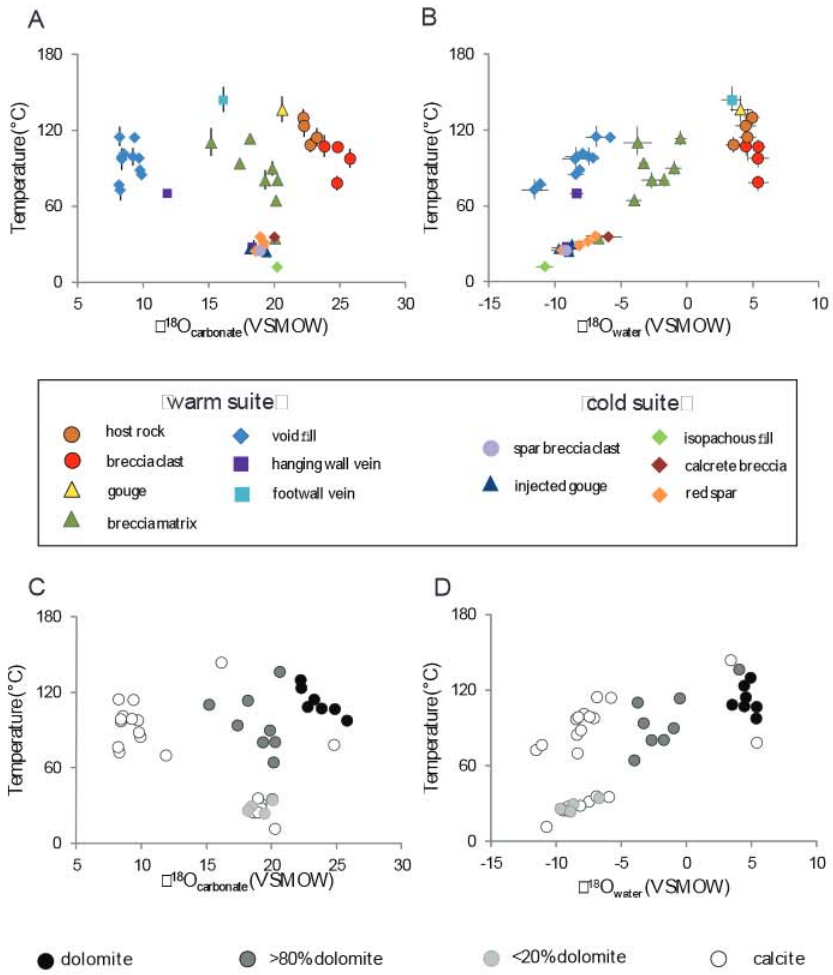

Fig. 5. Plots showing oxygen isotopic data and temperatures, keyed by texture (A and B) or by mineralogy (C and D). Textures in legend are grouped by approximate temperature. Errors in temperature and $\delta^{18}O_{water}$ are 1 sigma. One-sigma errors in oxygen isotopic compositions of the carbonates are smaller than the symbol size. Oxygen isotopic composition of the fluid is calculated from measured $\delta^{18}O$ and temperature of each sample (see text for discussion).

precipitated from water with $\delta^{18}O$ values of −11 to −6 permil (fig. 5B). This range in $\delta^{18}O$ (−9 ± 3‰) is typical of meteoric water in the region (fig. 1 in Horton and Chamberlain, 2006) and indistinguishable from water in equilibrium with void filling carbonate from the warm suite, which on average is about 60 °C warmer than the cold suite. Taken together, the composition of this suite suggests formation from a near-surface, meteoric water reservoir rich in low-$\delta^{13}C$ carbon. This set of compositions closely resembles those of soil carbonates, which contain carbon that is mainly sourced from oxidation of soil organic matter. Although the temperature of some samples might be higher than average surface temperatures in the region, previous studies

have suggested that clumped-isotope temperatures in soil carbonates could be recording relatively warm local soil temperatures during precipitation (for example Quade and others, 2007; Passey and others, 2010).

An important member of the cold suite is the calcite-spar breccia sample ES10-27 (fig. 3A) mentioned above. Although it is texturally similar to the other breccias, it is distinct in that (1) the clasts have a similar isotopic composition to the matrix, and (2) it is much colder and lighter in carbon. Additionally, this sample contains a significant component of sparry calcite clasts, and is only 20 percent dolomite. Notably, this sample is derived from the same locality in which fault gouge directly on the detachment (sample ES10-23) yielded a crystallization temperature of 130 °C. This sample most likely records a history of precipitation and subsequent fragmentation by the fault at near-surface conditions, although the possibility of recrystallization after brecciation cannot be ruled out, as discussed further below.

DISCUSSION AND CONCLUSIONS

Overall, the results reveal a wide range of precipitation temperatures (10 to 139 °C), with calculated $\delta^{18}O$ of pore waters as low as −11.6 permil (VSMOW) and $\delta^{13}C$ in carbonate as low as −8.0 permil (VPDB), indicating that the pore waters were meteoric. In general, $\delta^{18}O$ of breccia clasts, breccia matrix, and vein material are consistent with the results of Losh (1997) and Diehl and others (2010). Further, the temperatures of 70 to 115 °C recorded by the void-fill samples and hanging wall veins with $\delta^{13}C$ near 0 (that is, excluding the cold suite veins interpreted to have crystallized late), are similar to the 70 to 130 °C fluid inclusion homogenization temperatures obtained by Losh (1997) for veins in the hanging wall.

The temperatures of the void-fill samples are warmer than expected based on their relatively shallow depth of exhumation. As noted above, the structural thickness of the hanging wall is ~2000 m (fig. 1B). On the basis of extensive thermochronological data from the region (recently summarized in Fitzgerald and others, 2009 and Wernicke, 2011), the mid-Miocene geothermal gradient in the uppermost crust is 25 °C/km. The mid-Miocene mean surface temperature, based on clumped-isotope thermometry of lake deposits on the nearby Colorado Plateau was approximately 20 to 25 °C (Huntington and others, 2010). Using these parameters, the ambient temperature at 2000 m depth would have been only 70 to 75 °C. Although some of the warm suite samples overlap this range, most of them are much warmer. The difference suggests (1) the hanging wall blocks may have been much thicker than apparent from their relatively simple internal structure (for example, via thrust duplication), (2) the production of significant excess heat from friction along the fault (for example De Paola and others, 2011) and/or (3) the addition of heat from advection of warm pore fluid from depth up the detachment plane (for example Losh, 1997).

Although all three of these mechanisms may contribute heat, at present there is no evidence favoring major structural duplication in the hanging wall fault blocks, despite detailed geologic mapping of the entire allochthon (Wernicke and others, 1985; Shawe and others, 1988; Anderson and others, 2010). Thermal modeling of shear heating in carbonates suggests that the total amount of heat generated by friction is only sufficient to elevate temperatures within a few millimeters of the fault zone (for example, fig. 3A in Sulem and Famin, 2009), and thus friction is unlikely to be an important factor in raising ambient temperatures at meter scale away from the fault. Thus, if the upward advection of heat in meteoric pore fluids is the primary mechanism, the pore waters must have circulated to depths of at least 3 to 4 km in order to acquire sufficient heat.

The fluids from which void fills precipitated are meteoric, ruling out a direct contribution from any CO_2-rich (acidic) fluids of magmatic origin, as proposed by Diehl and others (2010). The Mormon Mountains, as any other mountain range in the

Basin and Range province, could overlie a pluton, a few kilometers below the present-day surface, which could provide a source of heat. Shawe and others (1988) suggested such a pluton may be present at depth, on the basis of (1) an aeromagnetic anomaly along the western flank of the range, and (2) the presence of a small igneous body (200 m^2) in the northern part of the range they interpreted to be an intrusive. However, the aeromagnetic anomaly is well correlated with the area where the Proterozoic crystalline basement is near the surface (near the center of the cross section in fig. 1C), and hence the age of any such subsurface intrusive is perhaps more likely to be Proterozoic than mid-Miocene. In a more detailed mapping study of the northern part of the range, Anderson and others (2010) mapped the same small igneous body as one of a number of exposures of a sequence of surface-accumulated andesite flows. Hence, although we cannot exclude a subsurface igneous body as a heat source, there is no clear evidence of Miocene intrusive activity in the range. The nearest magmatic center, the Kane Wash caldera, lies >30 km NNW of the study area. Thus if magmatic heat were driving convective flow of meteoric waters, it would be doing so on a grand scale.

For the "warm suite" of samples ($T > 60$ °C), high temperature samples are systematically lighter in carbon than low temperature samples (fig. 4B). To test the hypothesis that the trend is a result of equilibrium fractionation, and also to determine possible carbon sources, we calculated the carbon isotopic ratios of potential carbon sources: bicarbonate from dissolved carbonate, and CO_2 gas that could have resulted from decarbonation reactions. If the samples precipitated under equilibrium conditions from a single fluid, they will show a uniform $\delta^{13}C$ value (that is, no temperature dependence) for the relevant species of carbon. Using the fractionation factors from Mook and others (1974) and Bottinga (1968), we calculated the carbon isotopic composition of (1) bicarbonate ion and (2) CO_2 gas that would have been in equilibrium with each sample for the warm-suite void-fills, veins and gouge (fig. 6). Unexpectedly, the calculated ratios suggest rather large variation in $\delta^{13}C$ for bicarbonate (-0.6 to -5.1 permil), but relatively uniform $\delta^{13}C$ (-2.3 to -4.5 permil) for CO_2 gas (fig. 6), implying that this trend could be explained by buffering of carbon isotope compositions by a CO_2-rich fluid. This implication hinges on the assumption that the various carbonate textures all precipitated in equilibrium with a single fluid. If, however, we restrict the data to just the hanging wall veins and void fills, which are most likely to have precipitated from the same fluid, then the data suggest weak correlations with temperature for both CO_2 and bicarbonate ion (fig. 6, blue diamonds and purple squares only), and thus do not favor one over the other as a potential reservoir. A potential source for a reservoir of CO_2-rich fluid along the fault plane is thermal decomposition of carbonate, and so our results hint at the possibility that thermal decomposition might have taken place during slip on the detachment. On the other hand, analysis of fluid inclusions from these rocks suggests CO_2 was at most a minor component in the fluid system (Losh, 1997).

Our results do not provide any conclusive evidence, in terms of either textures or crystallization temperatures, for high-temperature thermal decomposition due to frictional heating within the slip zone, or subsequent recarbonation reactions. These reactions have been documented for at least one carbonate landslide (Hewitt, 1988), and are predicted on the basis of theoretical considerations and experimental data on large-slip seismogenic faults (for example Sulem and Famin, 2009; Han and others, 2010; De Paola and others, 2011). Because final crystallization of these very fine-grained materials could take place at relatively low temperatures, and because the final products of any high-temperature processes could be volumetrically minor, the data by no means rule out the possibility of thermal decomposition as an important process

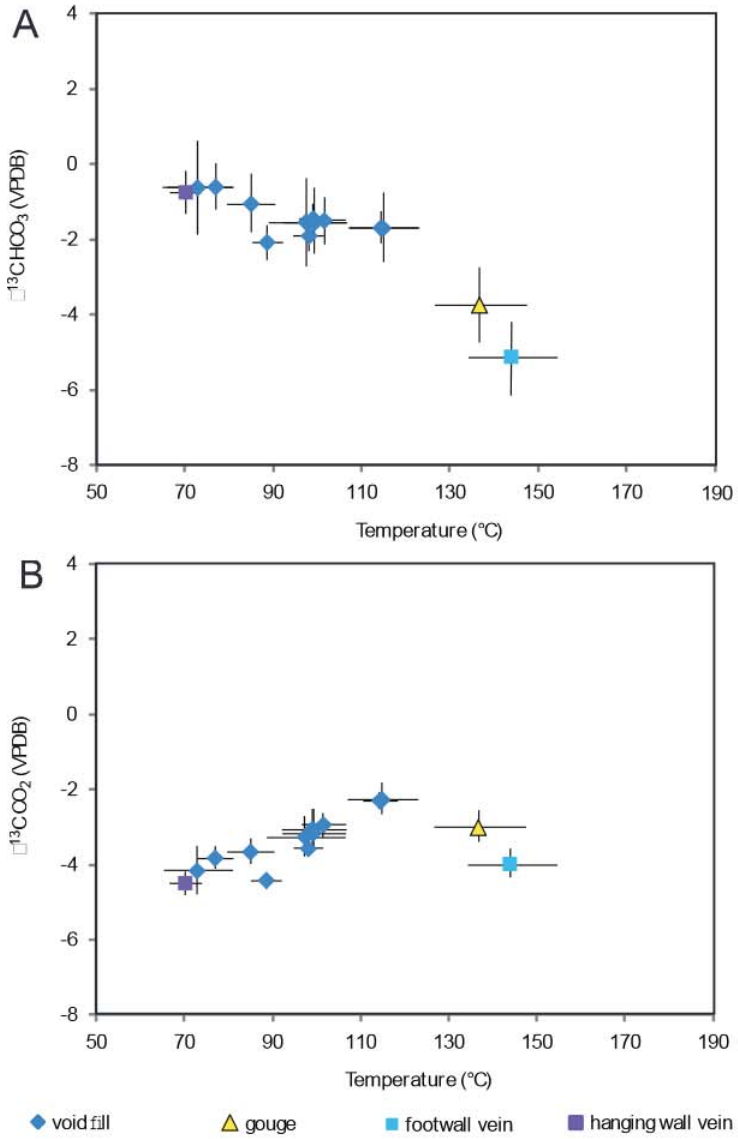

Fig. 6. Plots showing the $\delta^{13}C$ compositions of bicarbonate (A) and carbon dioxide (B) in equilibrium with void-filling carbonate, hot veins, and gouge. These values are calculated from each sample based on temperature and the $\delta^{13}C$ composition of the carbonate, assuming precipitation under equilibrium conditions (see text for discussion).

during slip. Our data at present, therefore, neither support nor exclude the possibility of thermal decomposition along the detachment.

Our data do not support earlier suggestions that the detachment is the base of one or more catastrophically emplaced landslides (Anders and others, 2006; Walker and

others, 2007). Anders and others (2006) concluded that there is no evidence of multiple deformation events within the fault zone. To the contrary, our results, as well as those of other observers, indicate a complex history of events. The evidence includes (1) multiple brecciation events (clasts within clasts within clasts) in the slip zone of the detachment (for example fig. 3B; Diehl and others, 2010, their fig. 4C), (2) sustained, high fluid temperatures (70 to 115 °C) at meter scale or greater within the fault zone (location 3, fig. 1; fig. 2C), (3) fragmentation recorded at temperatures as high as 135 °C and as low as 25 °C, with contrasting temperatures recorded in the same outcrop (for example, location 2, fig. 1; samples ES10-23 and ES10-27, respectively, table 1), (4) crosscutting veins in the hanging wall (Losh, 1997), and (5) the slow, syntectonic development of stylolites and veins in close association with faulting in the hanging wall (Anderson and others, 2010; Diehl and others, 2010). These data point toward the detachment as a single feature that developed over a significant amount of geologic time, in the presence of deeply circulating meteoric water (Losh, 1997; Anderson and others, 2010; Diehl and others, 2010; this study).

This study provides the first record of the apparent temperatures preserved by clumped-isotope thermometry in a suite of rocks as compared with their highly fragmented equivalents. Our finding that host rocks and breccia clasts are indistinguishable in apparent temperature suggests that natural fragmentation along faults does not reset the state of ordering of carbon and oxygen isotopes in carbonate ion groups, at least in ~8 mm clasts. Further, this method appears capable of preserving the record of precipitation events for very fine-grained samples, such as breccia matrix samples, through uplift and cooling of the rock mass, although it appears recrystallization can affect some samples, especially the fine-grained gouges. Another indication of the "memory" of the method is that both warm and cold temperatures are recorded by samples in the same outcrop. For example, whereas the gouge layer directly along the detachment records a temperature of 137 °C (ES10-23), a sample less than 1 m away in the hanging wall records precipitation temperatures in sparry calcite of less than 25 °C (ES10-27). The situation is reversed at another exposure, where the injected gouge from the cold suite lies within a meter of the warm void-fill calcite (samples ES09-05 and ES09-04, respectively).

Despite any clear textural evidence, it is nonetheless possible that some of the "cold suite" samples were originally warm, and have been recrystallized after emplacement, and thus their temperatures reflect low-temperature, fine-scale replacement and not the temperature of the preserved texture. Such fine-scale replacement, with relatively high temperature calcite (~94-123 °C), has recently been documented using clumped-isotope thermometry on fossil mollusks (Huntington and others, 2011). Low-temperature replacement probably occurred in the case of the injected gouge, because it is 97 percent calcite, but the host rock in the area is entirely dolostone. The injected gouge is also fine-grained, and very porous, which would facilitate recrystallization in the presence of post-deformational fluids.

However, other cold suite samples have textures that more likely result from deformation after crystallization. The best example of this is sample ES10-27, which contains a 5 mm clast that is both colder and lighter in carbon than the breccia matrix (25 °C vs. 35 °C, and −4.9‰ vs. −4.0‰). The matrix is 20 percent dolomite, but the clast is calcite (table 1). Unless somehow the coarser clasts were more readily replaced than the finer-grained matrix, it seems likely that the matrix contains a physical mixture of original, relatively warm dolomite and much colder, fine-grained calcite, whereas the clast contains only young, cold coarse-grained calcite. This suggests that brecciation occurred after the precipitation of the calcite spar in the clast.

The red calcite spar samples are more ambiguous, but are likely post-tectonic. Individual crystals are elongate and perpendicular to cavity boundaries, which show a

complicated structural pattern in hand specimen (fig. 3H). Close inspection does not reveal any evidence for post-crystallization fragmentation or tectonic strain. Hence we interpret this pattern as resulting from late precipitation of calcite spar along a complex system of void spaces in the host breccia.

This study demonstrates the utility of carbonate clumped-isotope thermometry in addressing structural problems. For example, without these analyses, it would be not be obvious that both the cold suite of samples and the much warmer void-fill samples precipitated from water with the same oxygen isotopic composition, about -9 ± 3 permil. This is especially true since both the oxygen and carbon isotopic compositions differ, and examples of each type of sample were collected within a few meters of each other. Clumped isotopes thus allow one to test hypotheses regarding different water sources (meteoric versus exchanged meteoric versus magmatic) and different temperatures independently.

ACKNOWLEDGMENTS

The clarity of the manuscript was greatly improved by the reviews of Lawford Anderson, Sam Haines, and an anonymous reviewer. This research was supported by NSF Grant EAR-0911772, and by the Gordon and Betty Moore Foundation. Tectonics Observatory contribution no. 168.

Appendix

Table A1

Clumped-isotope data, collected over four different analytical sessions. Analyses include samples for this study, heated gases and standards

Date	Sample ID	Voltage (mV)	$\delta^{13}C$ (VPDB)	$\delta^{13}C$ st. error	$\delta^{18}O$ gas	$\delta^{18}O$ st. error	δ_{47} (v. Oz)	δ_{47} st. dev	Δ_{47} (v. Oz)	Δ_{47} st. dev	Δ_{47} st. error	δ_{48} (v. Oz)	Δ_{48} (v. Oz)	Δ_{48} st. dev.
session 1														
11/9/2009	enriched BOC	15972	-9.954	0.001	57.604	0.001	26.126	0.071	0.002	0.026	0.009	133.496	64.722	2.607
11/9/2009	102-GC-AZ01	15948	0.474	0.001	24.377	0.001	3.215	0.050	-0.130	0.023	0.008	-2.464	-1.327	0.684
11/9/2009	E309-03 T1-S1	15966	1.125	0.001	16.555	0.001	-4.286	0.074	-0.452	0.047	0.017	-33.193	-17.159	0.703
11/10/2009	E309-03 T1-S2	15940	1.144	0.001	16.463	0.001	-4.369	0.061	-0.461	0.023	0.008	-33.698	-17.494	0.552
11/10/2009	ES09-04 T1-S1	15946	0.303	0.001	16.511	0.001	-5.199	0.059	-0.534	0.032	0.011	-33.074	-16.949	0.561
11/10/2009	E309-04 T1-S2	15962	0.295	0.001	16.683	0.001	-5.010	0.065	-0.508	0.042	0.015	-32.241	-16.434	0.399
11/10/2009	Carrera Hagit 1	15977	2.370	0.001	37.484	0.001	18.306	0.066	0.021	0.028	0.010	49.943	24.767	0.698
11/10/2009	heated BOC	11340	-8.951	0.001	27.937	0.001	-2.991	0.077	-0.756	0.041	0.015	5.688	-0.079	0.628
11/11/2009	ES09-04 T3-S1	15961	0.370	0.007	16.841	0.007	-4.780	0.056	-0.507	0.022	0.008	-35.057	-19.601	0.912
11/11/2009	ES09-04 T3-S2	15963	0.405	0.003	16.674	0.003	-4.913	0.074	-0.507	0.014	0.005	-34.940	-19.161	0.522
11/12/2009	enriched BOC	15932	-9.216	0.001	56.887	0.001	26.189	0.072	0.038	0.030	0.011	133.258	65.939	2.545
11/13/2009	ES090-05 T1-S1	15946	-7.219	0.000	26.844	0.000	-1.936	0.079	-0.295	0.033	0.012	8.046	4.391	0.449
11/13/2009	Carrera Hagit 1	15966	2.369	0.001	37.481	0.001	18.304	0.060	0.023	0.027	0.010	52.586	27.353	0.904
11/13/2009	ES09-02 T1-S1	8572	-0.282	0.002	29.633	0.002	7.739	0.093	-0.119	0.027	0.009	22.127	12.885	1.189
11/14/2009	ES09-02 T3-S1	15934	-0.188	0.002	29.755	0.002	7.928	0.055	-0.141	0.012	0.004	19.127	9.674	0.326
11/14/2009	enriched BOC	15945	-9.922	0.001	57.070	0.001	25.609	0.073	-0.018	0.051	0.018	131.824	64.226	3.063
11/15/2009	ES09-03 C1	15995	0.286	0.001	17.529	0.001	-4.155	0.066	-0.487	0.033	0.012	-30.288	-16.086	0.642
11/15/2009	ES09-03 M1	15951	0.305	0.001	17.660	0.001	-4.020	0.065	-0.502	0.015	0.005	-29.983	-16.030	0.639
11/15/2009	BW-83-X T5	15934	0.958	0.002	29.325	0.002	8.615	0.066	-0.137	0.027	0.010	17.081	8.482	0.734
11/15/2009	ES09-05 T3	15928	-6.655	0.001	26.552	0.001	-1.663	0.066	-0.278	0.030	0.011	5.685	2.605	0.616
11/15/2009	BW-83-X T6	15899	-0.785	0.001	34.484	0.001	12.140	0.068	-0.065	0.021	0.007	36.870	17.893	0.719
11/16/2009	102-GC-AZ01	15933	0.541	0.001	24.332	0.001	3.211	0.067	-0.155	0.026	0.009	-3.613	-2.392	0.658
session 2														
1/24/2010	enriched BOC	15951	-10.738	0.002	56.353	0.002	23.972	0.070	-0.141	0.043	0.015	121.691	56.094	3.030
1/25/2010	102-GC-AZ01	15971	0.464	0.001	24.416	0.001	3.246	0.068	-0.139	0.027	0.009	-1.541	-0.518	0.183
1/26/2010	E509-04 M1	15992	-0.062	0.002	18.006	0.002	-4.030	0.061	-0.515	0.016	0.006	-25.760	-12.454	0.561
1/26/2010	ES09-04 T4	15941	0.714	0.001	18.202	0.001	-3.044	0.066	-0.470	0.028	0.010	-25.226	-12.296	0.409
1/26/2010	ES09-01 T1	15917	0.053	0.003	26.938	0.003	5.227	0.060	-0.276	0.016	0.006	8.002	4.092	0.226
1/26/2010	Carrera Hagit 1	15978	2.362	0.001	37.577	0.001	18.319	0.050	-0.060	0.027	0.010	46.855	21.532	0.582
1/26/2010	ES09-01 T2	15904	-1.034	0.001	33.459	0.001	10.796	0.070	-0.154	0.037	0.013	30.967	14.067	0.641
1/26/2010	BOC	16002	-10.714	0.000	29.755	0.000	-2.968	0.070	-0.830	0.024	0.008	17.717	8.284	0.405
1/26/2010	ES09-01 T4	15989	0.559	0.003	24.736	0.003	3.452	0.066	-0.343	0.047	0.017	5.189	5.591	1.198

Table A1

(continued)

Date	Sample ID	Voltage (mV)	$\delta^{13}C$ (VPDB)	$\delta^{13}C$ st. error	$\delta^{18}O$ gas	$\delta^{18}O$ st. error	δ_{47} (v. Oz)	δ_{47} st. dev	Δ_{47} (v. Oz)	Δ_{47} st. dev	Δ_{47} st. error	δ_{48} (v. Oz)	Δ_{48} (v. Oz)	Δ_{48} st. dev.
session 2														
1/27/2010	ES09-04 C2	15926	-0.295	0.001	18.076	0.001	-4.172	0.079	-0.504	0.018	0.006	-26.153	-12.987	0.270
1/27/2010	ES09-02 T5	15944	-0.288	0.001	28.812	0.001	6.829	0.065	-0.214	0.043	0.015	14.366	6.758	0.259
1/27/2010	heated BOC	15988	-10.725	0.001	29.713	0.001	-3.016	0.056	-0.827	0.032	0.011	17.535	8.185	0.415
1/27/2010	Carrera Hagit 1	15968	2.361	0.002	37.579	0.002	18.350	0.061	-0.031	0.034	0.012	47.789	22.438	0.804
1/28/2010	enriched BOC	15922	-10.758	0.006	56.301	0.006	23.885	0.077	-0.157	0.040	0.014	120.974	55.523	2.869
1/28/2010	ES09-05 T5	15917	-5.105	0.001	27.847	0.001	1.193	0.081	-0.220	0.024	0.008	10.615	4.939	0.265
1/28/2010	ES09-01 T5	15906	-0.077	0.001	27.738	0.001	5.889	0.077	-0.286	0.020	0.007	10.840	5.355	0.254
1/28/2010	102-GC-AZ01	15969	0.575	0.001	24.268	0.001	3.177	0.080	-0.167	0.027	0.010	-2.110	-0.800	0.413
session 3														
05/24/2010	BOC	15941	-10.557	0.006	27.885	0.006	-4.684	0.070	-0.853	0.036	0.013	9.795	4.073	0.310
05/24/2010	102-GC-AZ01	15978	0.495	0.001	24.613	0.001	3.439	0.071	-0.172	0.030	0.011	-1.592	-0.954	0.174
05/25/2010	ES10-03	15952	-2.723	0.002	24.473	0.002	-0.100	0.058	-0.463	0.031	0.011	-2.360	-1.435	0.207
05/25/2010	ES10-08 T1	15944	-0.782	0.002	31.830	0.002	9.339	0.059	-0.233	0.024	0.008	23.814	10.208	0.360
05/26/2010	eBOC	15987	-10.679	0.004	59.557	0.004	27.228	0.066	-0.112	0.025	0.009	124.682	52.521	1.037
05/26/2010	Carrera	15973	2.336	0.008	37.703	0.008	18.356	0.080	-0.123	0.039	0.014	46.285	20.727	0.498
05/26/2010	ES10-05	15949	0.989	0.003	20.179	0.003	-0.716	0.063	-0.378	0.022	0.008	-16.776	-7.588	0.416
05/26/2010	ES10-15	15978	0.384	0.002	32.377	0.002	11.084	0.060	-0.168	0.024	0.008	26.072	11.361	0.440
05/26/2010	ES10-13	15971	-0.565	0.002	31.887	0.002	9.620	0.069	-0.220	0.033	0.012	24.278	10.555	0.443
05/26/2010	102-GC-AZ01	15947	0.448	0.003	24.409	0.003	3.211	0.066	-0.153	0.023	0.008	-1.849	-0.817	0.207
05/26/2010	ES10-06	15947	-0.917	0.002	32.880	0.002	10.294	0.063	-0.194	0.029	0.010	27.736	12.020	0.442
session 4														
5/25/2011	heated BOC	15917	-10.626	0.001	30.189	0.003	-2.550	0.021	-0.906	0.016	0.006	13.656	3.434	0.358
5/25/2011	TV01	15872	2.607	0.001	30.465	0.002	11.351	0.018	-0.134	0.033	0.012	14.676	3.848	0.398
5/25/2011	ES10-32 T1	15955	1.795	0.002	33.204	0.002	13.149	0.014	-0.281	0.034	0.012	22.358	6.103	0.585
5/25/2011	ES10-32 T2	15908	-8.022	0.002	28.416	0.003	-1.221	0.018	-0.350	0.034	0.012	9.621	2.874	0.476
5/26/2011	Carrera	15912	2.371	0.001	37.429	0.002	17.832	0.011	-0.381	0.021	0.007	33.898	9.194	0.318
5/26/2011	heated eBOC	15945	-10.957	0.001	51.287	0.002	18.199	0.015	-0.661	0.040	0.014	72.165	19.225	0.237
5/27/2011	ES10-35 T1	15879	-7.568	0.001	26.946	0.002	-2.211	0.028	-0.324	0.024	0.008	5.424	1.560	0.454
5/27/2011	ES10-35 T2*	15934	-7.052	0.002	27.541	0.001	-1.134	0.017	-0.336	0.052	0.018	7.309	2.275	0.573
5/27/2011	TV01	15912	2.609	0.002	30.451	0.004	11.311	0.014	-0.160	0.032	0.011	15.806	4.993	0.738
5/27/2011	ES10-27 T1	16025	-4.085	0.003	28.684	0.004	2.918	0.018	-0.295	0.042	0.015	11.199	3.901	0.706
5/27/2011	ES10-27 T2	15886	-4.926	0.002	27.322	0.006	0.758	0.019	-0.286	0.060	0.021	6.717	2.105	0.772
5/27/2011	ES10-21 T4	15918	-5.068	0.002	28.626	0.003	1.987	0.011	-0.215	0.030	0.011	10.083	2.911	0.659

TABLE A1

(continued)

Date	Sample ID	Voltage (mV)	$\delta^{13}C$ (VPDB)	$\delta^{13}C$ st. error	$\delta^{18}O$ gas	$\delta^{18}O$ st. error	δ_{47} (v. Oz)	δ_{47} st. dev	Δ_{47} (v. Oz)	Δ_{47} st. dev	Δ_{47} st. error	δ_{48} (v. Oz)	Δ_{48} (v. Oz)	Δ_{48} st. dev.
session 4														
5/28/2011	Carrera*	15888	2.350	0.016	37.464	0.024	17.920	0.020	-0.348	0.033	0.012	34.738	9.900	0.576
5/28/2011	heated BOC	15918	-10.841	0.001	29.330	0.002	-3.598	0.014	-0.899	0.026	0.009	11.700	3.168	0.340
5/29/2011	heated eBOC*	15949	-10.540	0.012	51.562	0.019	18.942	0.011	-0.634	0.019	0.007	75.347	21.677	0.412
5/30/2011	ES10-25 T3	15936	-5.345	0.001	27.531	0.003	0.542	0.023	-0.303	0.024	0.009	7.248	2.226	0.389
5/30/2011	ES10-25 T5	15942	-5.213	0.001	27.308	0.001	0.421	0.025	-0.331	0.035	0.012	8.121	3.531	0.267
5/30/2011	TV01	15869	2.569	0.001	30.454	0.003	11.298	0.020	-0.138	0.016	0.006	16.381	5.558	0.406
5/30/2011	heated BOC	15914	-10.651	0.001	28.800	0.003	-4.006	0.018	-0.968	0.039	0.014	10.748	3.255	0.732
5/30/2011	ES10-23 T5	15856	-1.447	0.002	30.153	0.004	6.779	0.015	-0.453	0.034	0.012	14.961	4.755	0.586
5/30/2011	ES10-22 T2	15880	-5.752	0.001	27.365	0.002	-0.010	0.019	-0.297	0.024	0.008	6.314	1.622	0.451
5/31/2011	ES10-33 T1	15943	-7.798	0.002	26.698	0.003	-2.697	0.019	-0.341	0.025	0.009	4.802	1.426	0.314

* Sample shows repaired value after an errant cycle was excluded from the δ_{47}, Δ_{47}, δ_{48}, and Δ_{48} analyses.

All oxygen isotopic ratios are with respect to VSMOW, all carbon isotopic ratios are with respect to VPDB. Sample values shown are uncorrected for heated gases and standards, which are applied separately for each session following Huntington and others (2009). Corrected values are presented in table 1.

References

Anders, M. H., Christie-Blick, N., and Walker, C. D., 2006, Distinguishing between rooted and rootless detachments: A case study from the Mormon Mountains of southeastern Nevada: The Journal of Geology, v. 114, n. 6, p. 645–664, http://dx.doi.org/10.1086/507612

Anderson, R. E., Felger, T. J., Diehl, S. F., Page, W. R., and Workman, J. B., 2010, Integration of tectonic, sedimentary, and geohydrologic processes leading to a small-scale extension model for the Mormon Mountains area north of Lake Mead, Lincoln County, Nevada: Geological Society of America Special Papers, v. 463, p. 395–426, http://dx.doi.org/10.1130/2010.2463(18)

Axen, G. J., Wernicke, B. P., Skelly, M. J., and Taylor, W. J., 1990, Mesozoic and Cenozoic tectonics of the Sevier thrust belt in the Virgin River Valley area, southern Nevada, *in* Wernicke, B., editor, Basin and Range extensional tectonics near the latitude of Las Vegas, Nevada: Geological Society of America Memoir, v. 176, p. 123–153.

Blanpied, M. L., Tullis, T. E., and Weeks, J. D., 1998, Effects of slip, slip rate, and shear heating on the friction of granite: Journal of Geophysical Research—Solid Earth, v. 103, n. B1, p. 489–511, http://dx.doi.org/10.1029/97JB02480

Bonifacie, M., Ferry, J. M., Horita, J., Vasconcelos, C., Passey, B. H., and Eiler, J. M., 2011, Calibration and applications of the dolomite clumped isotope thermometer to high temperatures: Mineralogical Magazine, v. 75, n. 3, p. 551.

Bottinga, Y., 1968, Calculation of Fractionation Factors for Carbon and Oxygen Isotopic Exchange in System Calcite-Carbon Dioxide-Water: Journal of Physical Chemistry, v. 72, n. 3, p. 800–808, http://dx.doi.org/10.1021/j100849a008

de Lorenzo, S., and Loddo, M., 2010, Effect of frictional heating and thermal advection on pre-seismic sliding: a numerical simulation using a rate-, state- and temperature-dependent friction law: Journal of Geodynamics, v. 49, n. 1, p. 1–13, http://dx.doi.org/10.1016/j.jog.2009.07.001

De Paola, N., Hirose, T., Mitchell, T., Di Toro, G., Viti, C., and Shimamoto, T., 2011, Fault lubrication and earthquake propagation in thermally unstable rocks: Geology, v. 39, n. 1, p. 35–38, http://dx.doi.org/10.1130/G31398.1

Diehl, S. F., Anderson, R. E., and Humphrey, J. D., 2010, Fluid flow, solution collapse, and massive dissolution at detachment faults, Mormon Mountains, Nevada: Geological Society of America Special Papers, v. 463, p. 427–441, http://dx.doi.org/10.1130/2010.2463(19)

Duvall, A. R., Clark, M. K., van der Pluijm, B. A., and Li, C. Y., 2011, Direct dating of Eocene reverse faulting in northeastern Tibet using Ar-dating of fault clays and low-temperature thermochronometry: Earth and Planetary Science Letters, v. 304, n. 3–4, p. 520–526, http://dx.doi.org/10.1016/j.epsl.2011.02.028

Eiler, J. M., 2007, "Clumped-isotope" geochemistry—The study of naturally-occurring, multiply-substituted isotopologues: Earth and Planetary Science Letters, v. 262, n. 3–4, p. 309–327, http://dx.doi.org/10.1016/j.epsl.2007.08.020

——— 2011, Paleoclimate reconstruction using carbonate clumped isotope thermometry: Quaternary Science Reviews, v. 30, n. 25–26, p. 3575–3588, http://dx.doi.org/10.1016/j.quascirev.2011.09.001

Fitzgerald, P. G., Duebendorfer, E. M., Faulds, J. E., and O'Sullivan, P., 2009, South Virgin–White Hills detachment fault system of SE Nevada and NW Arizona: Applying apatite fission track thermochronology to constrain the tectonic evolution of a major continental detachment fault: Tectonics, v. 28, p. TC2001, http://dx.doi.org/10.1029/2007TC002194

Goren, L., Aharonov, E., Sparks, D., and Toussaint, R., 2010, Pore pressure evolution in deforming granular material: A general formulation and the infinitely stiff approximation: Journal of Geophysical Research—Solid Earth, v. 115, p. B09216, http://dx.doi.org/10.1029/2009JB007191

Guo, W. F., Mosenfelder, J. L., Goddard, W. A., III, and Eiler, J. M., 2009, Isotopic fractionations associated with phosphoric acid digestion of carbonate minerals: Insights from first-principles theoretical modeling and clumped isotope measurements: Geochimica et Cosmochimica Acta, v. 73, n. 24, p. 7203–7225, http://dx.doi.org/10.1016/j.gca.2009.05.071

Haines, S. H., and van der Pluijm, B. A., 2010, Dating the detachment fault system of the Ruby Mountains, Nevada: Significance for the kinematics of low-angle normal faults: Tectonics, v. 29, p. TC4028, http://dx.doi.org/10.1029/2009TC002552

Han, R., Hirose, T., and Shimamoto, T., 2010, Strong velocity weakening and powder lubrication of simulated carbonate faults at seismic slip rates: Journal of Geophysical Research—Solid Earth, v. 115, p. B03412, http://dx.doi.org/10.1029/2008JB006136

Hausegger, S., Kurz, W., Rabitsch, R., Kiechl, E., and Brosch, F. J., 2010, Analysis of the internal structure of a carbonate damage zone: Implications for the mechanisms of fault breccia formation and fluid flow: Journal of Structural Geology, v. 32, n. 9, p. 1349–1362, http://dx.doi.org/10.1016/j.jsg.2009.04.014

Hewitt, K., 1988, Catastrophic landslide deposits in the Karakoram Himalaya: Science, v. 242, n. 4875, p. 64–67, http://dx.doi.org/10.1126/science.242.4875.64

Hirose, T., and Shimamoto, T., 2005, Slip-weakening distance of faults during frictional melting as inferred from experimental and natural pseudotachylytes: Bulletin of the Seismological Society of America, v. 95, n. 5, p. 1666–1673, http://dx.doi.org/10.1785/0120040131

Horton, T. W., and Chamberlain, C. P., 2006, Stable isotopic evidence for Neogene surface downdrop in the central Basin and Range Province: Geological Society of America Bulletin, v. 118, n. 3–4, p. 475–490, http://dx.doi.org/10.1130/B25808

Huntington, K. W., Eiler, J. M., Affek, H. P., Guo, W., Bonifacie, M., Yeung, L. Y., Thiagarajan, N., Passey, B., Tripati, A., Daeron, M., and Came, R., 2009, Methods and limitations of "clumped" CO2 isotope (Δ_{47}) analysis by gas-source isotope ratio mass spectrometry: Journal of Mass Spectrometry, v. 44, n. 9, p. 1318–1329, http://dx.doi.org/10.1002/jms.1614

Huntington, K. W., Wernicke, B. P., and Eiler, J. M., 2010, Influence of climate change and uplift on

Colorado Plateau paleotemperatures from carbonate clumped isotope thermometry: Tectonics, v. 29, p. TC3005, http://dx.doi.org/10.1029/2009TC002449
Huntington, K. W., Budd, D. A., Wernicke, B. P., and Eiler, J. M., 2011, Use of clumped-isotope thermometry to constrain the crystallization temperature of diagenetic calcite: Journal of Sedimentary Research, v. 81, n. 9, p. 656–669, http://dx.doi.org/10.2110/jsr.2011.51
Losh, S., 1997, Stable isotope and modeling studies of fluid-rock interaction associated with the Snake Range and Mormon Peak detachment faults, Nevada: Geological Society of America Bulletin, v. 109, n. 3, p. 300–323, http://dx.doi.org/10.1130/0016-7606(1997)109(0300:SIAMSO)2.3.CO;2
McCaig, A. M., Wayne, D. M., Marshall, J. D., Banks, D., and Henderson, I., 1995, Isotopic and fluid inclusion studies of fluid movement along the Gavarnie thrust, central Pyrenees—Reaction fronts in carbonate mylonites: American Journal of Science, v. 295, p. 309–343, http://dx.doi.org/10.2475/ajs.295.3.309
Mook, W. G., Bommerson, J. C., and Staverman, W. H., 1974, Carbon isotope fractionation between dissolved bicarbonate and gaseous carbon-dioxide: Earth and Planetary Science Letters, v. 22, n. 2, p. 169–176, http://dx.doi.org/10.1016/0012-821X(74)90078-8
O'Neil, J. R., Clayton, R. N., and Mayeda, T. K., 1969, Oxygen isotope fractionation in divalent metal carbonates: Journal of Chemical Physics, v. 51, p. 5547–5558, http://dx.doi.org/10.1063/1.1671982
Passey, B. H., Levin, N. E., Cerling, T. E., Brown, F. H., and Eiler, J. M, 2010, High-temperature environments of human evolution in East Africa based on bond ordering in paleosol carbonates: Proceedings of the National Academy of Sciences of the United States of America, v. 107, n. 25, p. 11245–11249, http://dx.doi.org/10.1073/pnas.1001824107
Quade, J., Garzione, C., and Eiler, J., 2007, Paleoelevation reconstruction using pedogenic carbonates, *in* Kohn, M., editor, Paleoaltimetry: Geochemical and Thermodynamic approaches: Reviews in Mineralogy and Geochemistry, v. 53–87, http://dx.doi.org/10.2138/rmg.2007.66.3
Rice, J. R., 1992, Chapter 20 Fault stress states, pore pressure distributions, and the weakness of the San Andreas fault, *in* Brian, E., and Teng-fong, W., editors, Fault Mechanics and Transport Properties of Rocks—A Festschrift in Honor of W. F. Brace: International Geophysics, v. 51, p. 475–503, http://dx.doi.org/10.1016/S0074-6142(08)62835-1
——— 2006, Heating and weakening of faults during earthquake slip: Journal of Geophysical Research—Solid Earth, v. 111, p. B05311, 29 p., http://dx.doi.org/10.1029/2005JB004006
Rosenbaum, J., and Sheppard, S. M. F., 1986, An isotopic study of siderites, dolomites and ankerites at high temperatures: Geochimica et Cosmochimica Acta, v. 50, n. 6, p. 1147–1150, http://dx.doi.org/10.1016/0016-7037(86)90396-0
Schauble, E. A., Ghosh, P., and Eiler, J. M., 2006, Preferential formation of ^{13}C—^{18}O bonds in carbonate minerals, estimated using first-principles lattice dynamics: Geochimica et Cosmochimica Acta, v. 70, n. 10, p. 2510–2529, http://dx.doi.org/10.1016/j.gca.2006.02.011
Shawe, D. R., Blank, H. R., Jr., Wernicke, B. P., Axen, G. J., Barton, H. N., Day, G. W., and Rains, R. L., 1988, Mineral Resources of the Mormon Mountains Wilderness Study Area, Lincoln County, Nevada: U.S. Geological Survey Bulletin, v. 1729-B, p. B1–B18.
Sibson, R. H., 1975, Generation of pseudotachylyte by ancient seismic faulting: Geophysical Journal of the Royal Astronomical Society, v. 43, n. 3, p. 775–794, http://dx.doi.org/10.1111/j.1365-246X.1975.tb06195.x
Sulem, J., and Famin, V., 2009, Thermal decomposition of carbonates in fault zones: Slip weakening and temperature-limiting effects: Journal of Geophysical Research, v. 114, B03309, http://dx.doi.org/10.1029/2008JB006004
Vasconcelos, C., McKenzie, J. A., Warthmann, R., and Bernasconi, S. M., 2005, Calibration of the $\delta^{18}O$ paleothermometer for dolomite precipitated in microbial cultures and natural environments: Geology, v. 33, n. 4, p. 317–320, http://dx.doi.org/10.1130/G20992.1
Walker, C. D., Anders, M. H., and Christie-Blick, N., 2007, Kinematic evidence for downdip movement on the Mormon Peak detachment: Geology, v. 35, n. 3, p. 259–262, http://dx.doi.org/10.1130/G23396A.1
Wernicke, B., 2011, The California River and its role in carving Grand Canyon: Geological Society of America Bulletin, v. 123, n. 7–8, p. 1288–1316, http://dx.doi.org/10.1130/B30274.1
Wernicke, B., Walker, J. D., and Beaufait, M. S., 1985, Structural discordance between Neogene detachments and frontal Sevier thrusts, central Mormon Mountains, Southern Nevada: Tectonics, v. 4, n. 2, p. 213–246, http://dx.doi.org/10.1029/TC004i002p00213